

PACS numbers: 96.60.\_j, 84.60.Jt

## AN EFFECTIVE MODELING APPROACH FOR HIGH EFFICIENT SOLAR CELL USING VIRTUAL WAFER FABRICATION TOOLS

***Khomdram Jolson Singh, Subir K. Sarkar***

Jadavpur University,  
Raja S.C. Mullick Road, 700032, Kolkata, India  
E-mail: [jolly4u2@rediffmail.com](mailto:jolly4u2@rediffmail.com)

*In order to give a real understanding and realization of all the phenomena occurring inside the photovoltaic cell devices, the development of a reliable simulated model first is also essential. In this paper, a novel method for developing a realistic model of an efficient solar cell is presented. An efficient model of a Dual Junction InGaP/GaAs solar cell having GaAs tunnel diode is prepared and fully simulated using Silvaco VWF/ATLAS code. An optimization of window layer, ARC, BSF etc are also performed incorporating the effect of some of the different parameters on the performance of this model. The major stages of the process are explained and the simulation results are compared with published experimental data to demonstrate the accuracy of our results produced by the model utilizing this technique. For this optimized InGaP/GaAs Dual Junction cell model having 125 nm DLAR on 18 nm InAlP textured window with effective 500 nm InAlGaP bottom BSF, a maximum conversion efficiency of 32.20 % (1 sun) and 36.67 % (1000 suns) is obtained under AM1.5G illumination. The introduction of this modeling technique to the photovoltaic community will prove to be of great importance in aiding in the design and development of advanced solar cells using Silvaco Virtual Wafer Fabrication Tools.*

**Keywords:** VIRTUAL WAFER FABRICATION, ATLAS, ANTI REFLECTIVE COATING, EFFICIENCY, DUAL-JUNCTION.

*(Received 04 February 2011, in final form 14 October 2011)*

### 1. INTRODUCTION

The virtual wafer fabrication package (VWF) is one of the major products from the Silvaco software package. Silvaco TCAD is a simulation software tool targeting the area of electronic design [1]. This is a large suite of highly sophisticated tools that aid in the design and development of all types of semiconductor and VLSI devices starting from simple bipolar transistors to advanced memory devices. The modeling starts from simple electrical conductivity and extend to thermal analysis, radiation, optical losses etc. The ability to incorporate the various detailed layer growth processes and material properties such as mobilities, recombination parameters, ionization coefficients, optical parameters, etc in VWF model, add to the accuracy of the simulation. All these critical capabilities are vital in the design and fabrications of state-of-the-art solar cells. Even though circuit modeling of solar cells is popular [2], however, the effort from researchers in the photovoltaic field, or from solar cell manufacturers, to utilize this powerful tool for the modeling and optimization of advanced multi-function cells is still a long way to go. In this paper, our successful effort in developing an efficient multi-junction solar cell model is introduced.

## 2. THE SOLAR CELL MODELING

In order to model and build a state-of-the-art multi-junction cell, it was necessary to start with individual simple cells of well known characteristics, and established performances to verify the accuracy and capability of this technique. That way, their efficiency could be optimized and their performance characteristics could be compared with the results reported in the literature [3-5].

A detailed set of major material parameters shown in Table 1 used in our design has been produced by literature research and calculations as well as calibration from well-known cells [6, 7]. A schematic of this model with detailed thickness and doping profile is designed in Fig. 1.

*Table 1 – Major Parameter used in this design*

Material	GaAs	InAlP	InGaP	InAlGaP
Band gap $E_g$ [eV] @ 300 K	1.42	2.4	1.9	2.3
Lattice constant $a$ [Å]	5.65	5.65	5.65	5.65
Permittivity $\epsilon_s/\epsilon_0$	13.1	11.7	11.6	11.7
Affinity [eV]	4.07	4.2	4.16	4.2

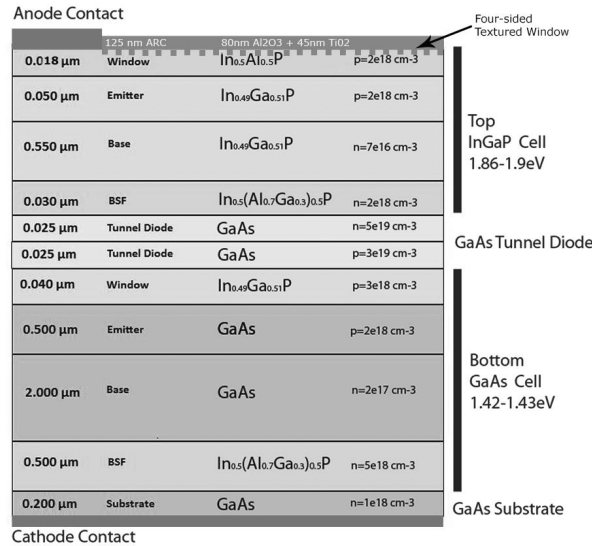


*Fig. 1 – Schematic diagram of this cell model*

### 2.1 Mesh Generation

The first step in modeling the device is specifying the mesh on which the device will be constructed shown in Fig. 2. This can be 2D or 3D and can be comprised of many different sections. Orthogonal and cylindrical coordinate systems are available. Several constant or variable densities can be specified while scaling and automatic mesh relaxation can also be used. This way, a number of minimum triangles are created; this determines the resolution of the simulation. Mesh design is an important factor to consider when designing semiconductors in SILVACO ATLAS<sup>TM</sup>. The mesh intersections are designed by the simulation program to sufficiently cover the constructed

device and are the data extraction points used to sample electrical characteristics of the model at designated intervals. It is often the requirement for accuracy and numerical efficiency that dictate the size of the sample intervals. Examining Fig. 2, it is seen that the entire structure is thoroughly sampled at designated intervals.

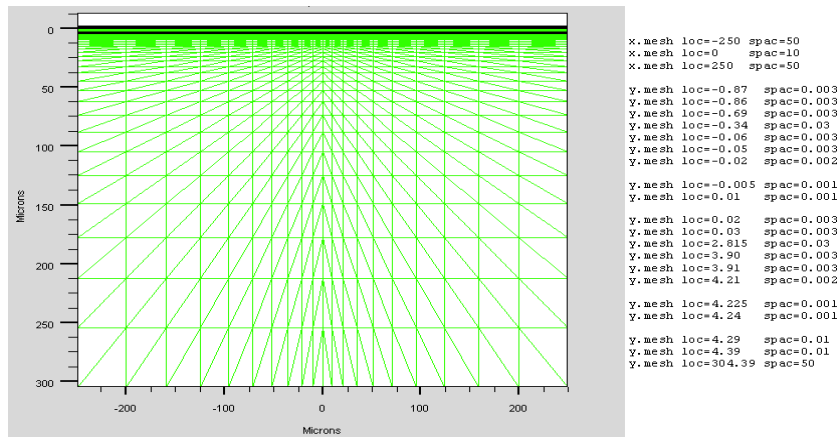


*Fig. 2 – Solar Cell Mesh Model*

Depending on the complexity of device design, some areas may require more sampling than others to sufficiently sample all the electrical activity created by the recombination and generation processes occurring within the device. Accuracy increases with finer grid points while numerical efficiency

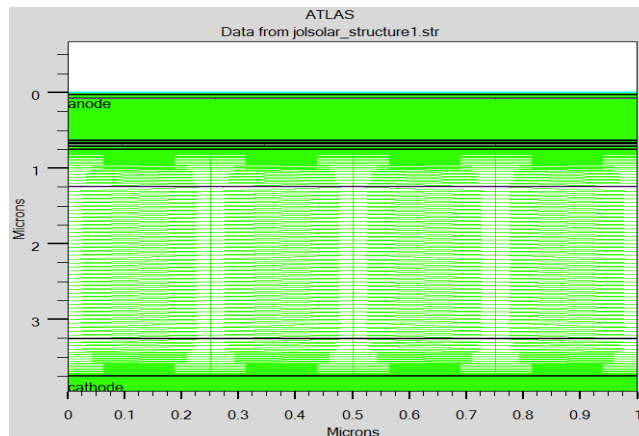


*Fig. 3 – Our design with finer mesh model*

increases with fewer grid points. Since these simulations are computer driven programs, a finer grid equates to longer simulation runtime. As mentioned for the solar cell, examining the above device it is seen that the structure is thoroughly sampled at designated intervals. The objective was straightforward; electrically sample the devices effectively but refrain from over-sampling, resulting in long and unnecessary simulation runtime. Therefore, in Fig. 3, finer mesh are defined in more critical areas (junction, quantum well, tunneling region etc) only rather than the whole cell.

## 2.2 Material Specification

A library of materials is a part of the ATLAS tool. Many common materials can be selected from this library for use in defining material properties. Since solar cells are using state-of-the-art materials that may not be listed in the library, ATLAS has the ability to fully define new materials. A minimum set of property data must be specified for a new material to include band gap, dielectric constant, electron affinity, densities of conduction and valence states, mobilities, recombination coefficient, and an optical file containing refractive indices  $n$  and extinction coefficients  $k$  for a material [8]. The optical file determines the transmission and attenuation of light as it passes through the semiconductor.

As an example in our code “*material mat = InAlGaP sopra = Againp7.nk*”

## 2.3 Doping Specification

Each region with a semiconductor material is allocated a type and level of doping concentration. Doping can either be n or p type with a choice of uniform, linear, or Gaussian distribution. The concentration is in units of impurities per cubic centimeter.

## 2.4 Model Specification

ATLAS permits the user to identify a variety of models for calculating carrier mobility and recombination. The Concentration-Dependent Low Field Mobility model (CONMOB) was used to model the doping-dependent low-field mobilities of electrons and holes in GaAs at 300 K. The recombination models utilized were the Optical Recombination (OPTR) and the Shockley-Read-Hall (SRH) recombination models. SRH recombination model takes into account the electrons being emitted or captured by donor and acceptor-like traps. The OPTR determines the possibility that a photon is generated when an electron and hole recombined. Green has shown that the OPTR model increase the accuracy of the solar cell simulation.

We used SRH FERMI CONMOB OPTR AUGER BGN model in our design.

## 2.5 Light Specification

ATLAS luminous optical-electric simulation module has the ability to determine photogeneration at each mesh point, thus a number of light sources can be simulated with various changes in their location, orientation, and intensity.

## 2.6 Solve Specification

After defining all input parameters, ATLAS can use various methods to solve for output data. Various numerical methods can be used to solve the cell parameters. The resulting solutions then can be used to generate  $I_{sc}$ ,  $V_{oc}$ , and cell efficiency, along with representative I-V curves and frequency responses. For this thesis, solutions of efficiency and plots of the I-V curves were used extensively.

## 3. SIMULATION RESULT

Following the above cited steps, and similar to the actual processes during the fabrication of a solar cell, only the p-n junction was built on the substrate using the proper doping concentration of the actual comparable cell. The back

surface field (BSF) layer, which is used to enhance cell efficiency, was then added and the improvement on the device performance was observed. Buffer and window layers along with the metal grid and contacts were the final additions to the individual simple cells. The corresponding typical ATLAS cell models is shown in Fig. 4. It is a two-dimensional, virtual-view of the constructed solar cell model. Since the cell's dimensions can be specified in SILVACO ATLAS™, this device was modeled to represent an actual solar cell. ATLAS uses a mathematical model that operates on any semiconductor device. This model consists of a set of fundamental equations which link together the electrostatic potential and carrier densities [1]. Fig. 5 is a close up depiction of the n-p junction to represent the differences in concentrations i.e. doping profile.

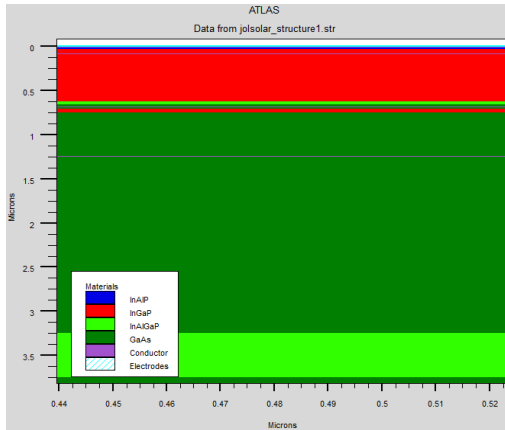


**Fig. 4** – ATLAS model of this InGaP/GaAs DJ Cell

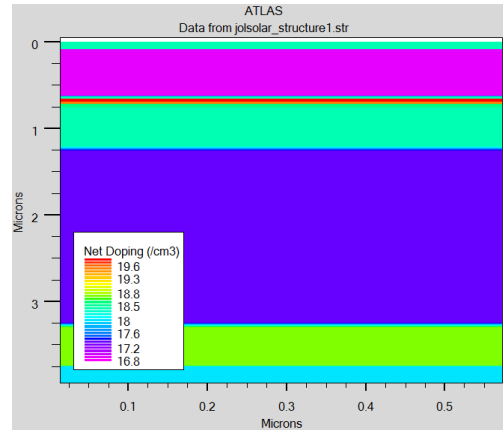


**Fig. 5** – Doping profile of this model

Even though any type of solar spectrum and photon concentration can easily be specified and used, for the purposes of this paper, a standard 1 sun AM1.5G as shown in Fig. 6 will be used as an example light source to illuminate the cell models developed using the SILVACO/ATLAS package.

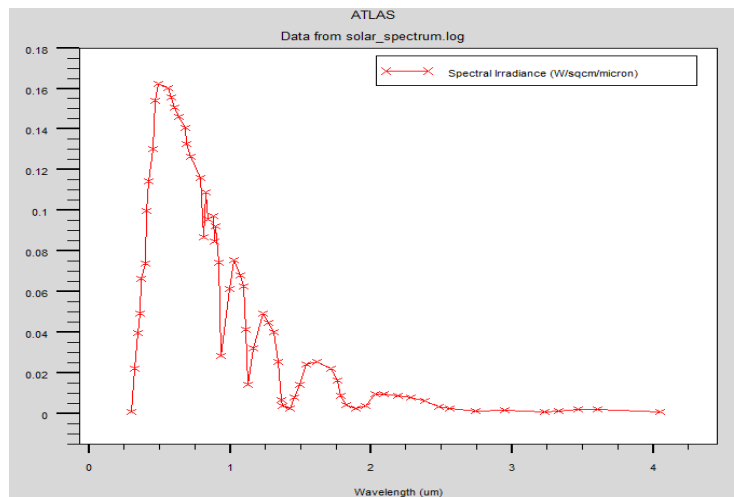


**Fig. 6** – AM1.5G spectrum used to illuminate the model

Fig. 7 illustrates the SILVACO ATLAS™ solar cell model results with photogeneration rate. The legend within the figure defines the solar cell's photogeneration rates. These are expressed using the log of the electron-hole pair generation rates that correspond to the color-coded display. For example the highest numerical value (e.g., 21.6) corresponds to the color-coded horizontal layer that is generating  $10^{21.6}$  electron-hole pairs per  $\text{cm}^3$ . The very top portion of the vertical-band seen spanning the model represents the upper metal contact of the semiconductive material. The thin strip along the horizontal bottom of the cell is the lower metal contact. The top and bottom metal contacts of the device are more appropriately termed as the anode and cathode, respectively. These areas identify the power extraction points of the solar cell.

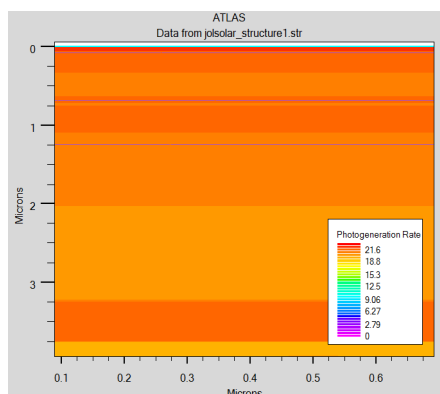


**Fig. 7** – Photogeneration Rate generated in this model

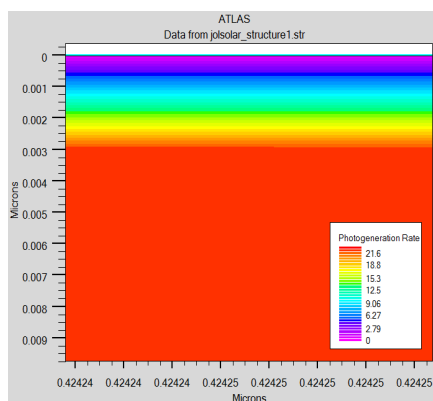


**Fig. 8** – Photogeneration Rate showing closer top layer

SILVACO ATLAS™ also allows the user to zoom in on model areas, enabling its users to examine specific regions of constructed models. Fig. 8 shows a closer examination of device operation near the surface of the solar cell. As seen in the figure, this closer view better illustrates the upper metal contact of the semiconductive material that is outlined by the light-blue, rectangular shaped region at the very top-center of the device. This closer examination also reveals that the photogeneration rate is significantly less directly beneath this metal contact region of the solar cell than the other regions. This is because the area directly beneath the electrical contact is blocked from the simulated solar light. Most of the higher photogeneration rates are observed in the upper solar cell layers because a significant majority of the photon energy is absorbed here prior to reaching the remaining body (e.g., the yellow region) of the simulated device. This can be verified from Fig.9 that shows the generation of higher cathode current in ultraviolet and visible part of the spectrum i.e. obviously in top InGaP cell design with a bandgap of 1.85 eV.

Various parameters distributed properly throughout its area provide a very valuable insight. Such parameters include potential, electron and hole concentrations, electron and hole current densities, photogeneration rates and electrostatic fields. Using the data generated by the illuminated model, short-circuit currents and open-circuit voltages were obtained. I – V curves and spectral responses were also produced from the model under AM1.5G and plotted. Dark current of the model were found to correspond to that of previously reported data [6].

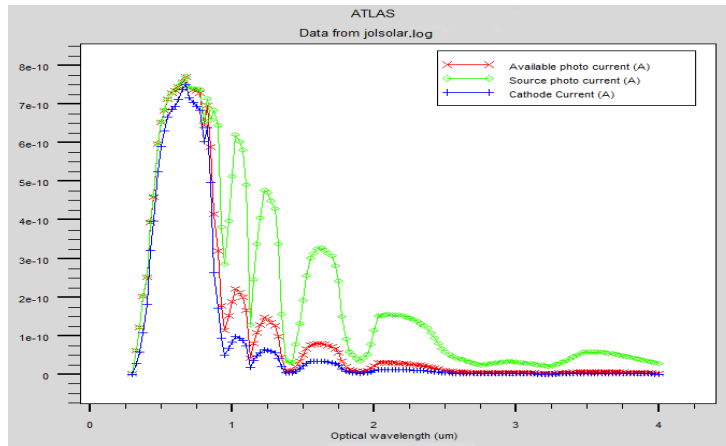


Fig. 9 – Cathode current generated in the model

4. MAJOR SOLAR CELL DEVICE PERFORMANCE PARAMETERS

Fig. 10 show various comparison of this textured window with other standard layers used in the literature. The reflectivity of a window layer is given as

$$R(\lambda) = \frac{(n(\lambda) - 1)^2 + k(\lambda)^2}{(n(\lambda) + 1)^2 + k(\lambda)^2}$$

Here, using Double layer anti-reflective coating, DLAR (80 nm Al<sub>2</sub>O<sub>3</sub> /45 nm TiO<sub>2</sub>) on 18 nm textured InAlP window greatly reduced the reflection losses thereby enhancing absorption and photocurrent of the cell. This type of optical simulation result can be accurately simulated in ATLAS with various window structures.

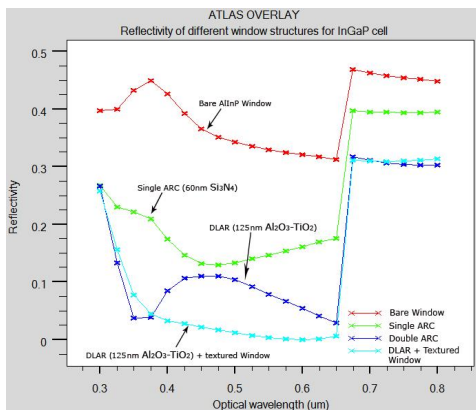


Fig. 10 – Reflectance on window layer using different ARC system for loss optimization

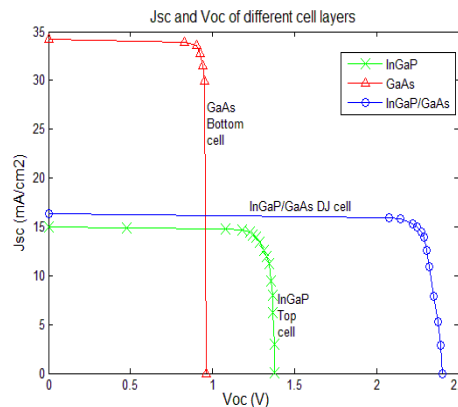


Fig. 11 – I – V characteristics of individual and complete cell

The following important performance equation is incorporated in the simulation design code to get our desired output result from the model. One of the I–V characteristic plot is shown in Fig. 11.

$$I = I_0 \left[ \exp\left(\frac{qV}{nKT}\right) - 1 \right] - I_L,$$

where  $I_L$  = light generated current.

The equation for the I-V curve in the first quadrant is:

$$I = I_0 \left[ \exp\left(\frac{qV}{nKT}\right) - 1 \right]$$

The open – circuit voltage,  $V_{oc}$ , is the maximum voltage available from a solar cell, and this occurs at zero current.

$$V_{oc} = \frac{nKT}{q} \ln\left(\frac{I_L}{I_0} + 1\right)$$

The short-circuit current and the open-circuit voltage are the maximum current and voltage respectively from a solar cell. As FF is a measure of the "squareness" of the I-V curve, a solar cell with a higher voltage has a larger possible FF since the "rounded" portion of the I-V curve takes up less area. A more commonly used expression for the FF can be determined empirically as:

$$FF = \frac{V_{oc} - \ln(V_{oc} + 0.72)}{V_{oc} + 1}$$

The efficiency of a solar cell is determined as the fraction of incident power (Terrestrial solar cells are measured under AM1.5 conditions) which is converted to electricity and is defined as:

$$P_{max} = V_{oc} I_{sc} FF$$

Therefore efficiency of a solar cell is given by

$$\eta = \frac{V_{oc} I_{sc} FF}{P_{in}}$$

where  $V_{oc}$  is the open-circuit voltage,  $I_{sc}$  is the short-circuit current,  $FF$  is the fill factor,  $\eta$  is the efficiency, and  $P_{in}$  is the input power.

## 5. COMPARISON OF RESULTS WITH EXPERIMENTAL DATA

We observed that the performance and results produced from this virtually fabricated MJ model, is very similar to those published in Ref. [3] as well as in many other papers [4-6]. The results are also comparable to experimental data of similar manufactured cells. The results compared favorably with corresponding experimental data for similar devices using the same parameters. Minor differences are only due to the variations in the material and optical parameters used. If needed, those can easily be tuned to reflect experimental results more accurately. The expected generated I-V characteristics can be seen in Fig. 12, and demonstrate the close agreement to the experimental results of the Spectrolab MJ cell [3].



Table 2 shows the various comparisons of this optimized design with other previous findings and found the result of this simulation model gives good result with high efficient performance than other proposed in various literatures [11, 12].

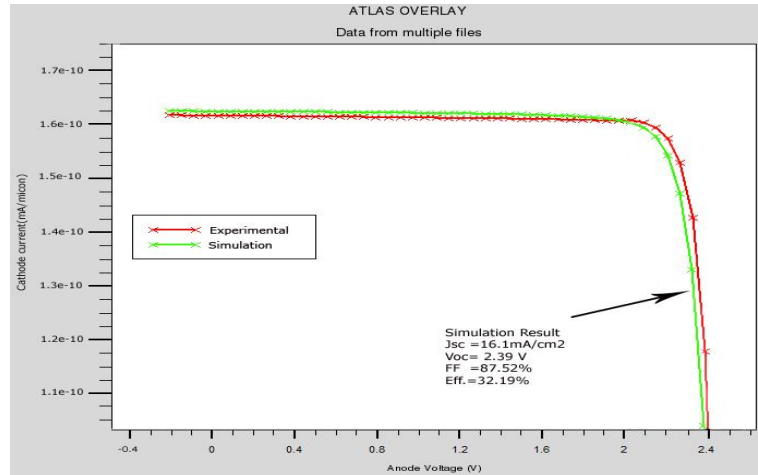


**Fig. 12** – Comparison of this DJ model generated IV characteristics with experimental results

**Table 2** – Comparison of the different optimized InGaP/GaAs DJ solar cell structures

Solar cells	Spectrum	Sun	$V_{oc}$ (V)	$J_{sc}$ (mA/cm <sup>2</sup> )	FF (%)	Conv. eff. (%)
DJ InGaP/GaAs solar cell Ref. (Lueck et al. 2006)[11]	AM1.5G	1	2.32	10.9	79.00	23.6
DJ InGaP/GaAs solar cell Ref.(J. W. Leem et al. 2010) [12]	AM1.5G	1	2.30	10.6	87.55	25.14
This Optimized DJ InGaP/GaAs Solar cell model	AM1.5G	1	2.39	16.1	87.52	32.20
Same model	AM1.5G	1000	2.66	160.9	89.50	36.67

## 6. OPTIMIZATION

To demonstrate the capability of this developed MJ model, an example of an optimization process is presented. In order to maximize cell efficiency, a search for the optimum cell layers thickness was conducted [9]. As expected, the results demonstrated in Fig. 11 verified some of the parameters and data of current MJ cell designs that were previously obtained through years of research, experimentation and fabrication. Effects of other cell parameters, such as doping level, different band gap materials and others were also researched. A detailed novel general optimization approach using genetic algorithm for multi-junction cells design, along with the development of a state-of the-art quad-junction cell is presented in another publication [10]. Here in this paper, two BSF materials (i.e. AlGaAs, InAlGaP) with their

varied thickness (i.e. 0.05, 0.1, 0.5, 1.0)  $\mu\text{m}$  both for top and bottom cells are investigated for high  $V_{oc}$  and found that the maximum  $J_{sc} = 16.10 \text{ mA/cm}^2$ ,  $V_{oc} = 2.392 \text{ V}$  with 32.2 % efficiency is optimized with InAlGaP 30 nm Top cell BSF and 500 nm bottom cell BSF. And window layer is passivated with DLAR using  $\text{Al}_2\text{O}_3/\text{TiO}_2$  on textured surface. Current matching between the top and bottom cell is done by 25 nm GaAs Tunnel diode.

## 7. CONCLUSIONS

A virtual fabrication technique has been presented for modeling and developing high efficient multi-function solar cells. The developed models have demonstrated the effects of various material parameter on many of the cell characteristics. Simulation and modeling of different band gap material and compounds can also be incorporated, and currently underway. In our opinion, the introduction of this modeling technique predicts the various effect of window material, layer structure, ARC, BSF etc on cell optical and electrical performance can be studied for further enhancement. The research conducted for this work concludes that the SILVACO ATLAS<sup>TM</sup> Virtual Wafer Fabrication software could be offered as a valid substitution for future high efficient solar cell design tool prior to the real fabrication process.

## REFERENCES

1. Silvaco ATLAS (vol. I&II) user's manual, Silvaco International.
2. E. Van Kerschaver, J. Nijs, R. Mertens, M. Ghannam, Conference Record of the 26th IEEE – *Photovoltaic Specialists Conference*, 175 (1997).
3. R.R. King, N.H. Karam, J.H. Ermer, N. Haddad, P. Colter, T. Isshiki, H. Yoon, H.L. Cotal, D.E. Joslin, D.D. Krut, R. Sudharsanan, K. Edmondson, B.T. Cavicchi, D.R. Lillington, Conference Record of the 28th IEEE 2000 – *Photovoltaic Specialists Conference*, 998 (2000).
4. D. Lillington, H. Cotal, J. Ermer, D. Friedman, T. Moriarty, A. Duda, IECEC 35th Intersociety – *Energy Conversion Engineering Conference and Exhibit*, 1, 516 (2000).
5. N.H. Karam, R.R. King, B.T. Cavicchi, D.D. Krut, J.H. Ermer, M. Haddad, C. Li, D.E. Joslin, M. Takahashi, J.W. Eldredge, W.T. Nishikawa, D.R. Lillington, B.M. Keyes, R.K. Ahrenkiel, Spectrolab Inc., C.A. Sylmar, *IEEE T. Electron Dev.* **46**, 2116 (1999).
6. I. Vurgaftman, J.R. Meyer, L.R. Ram-Mohan *J. Appl. Phys.* **89**, 5815 (2001).
7. SILVACO Data Systems Inc.: *Silvaco ATLAS User's Manual* (2009).
8. SOPRA. <http://www.sopra-sa.com> (2009) Accessed (15 june 2010).
9. S. Michael, P. Michalopoulos, *The 45 Midwest Symposium on Circuits and Systems – Tulsa, Oklahoma, Aug 5–7*, (2000).
10. S. Michael, A. Bates, *Sol. Energ. Mat. Sol. C.* **87**, 771 (2005).
11. M.R. Lueck, C.L. Andre, A.J. Pitera, M.L. Lee, E.A. Fitzgerald, S.A. Ringel, *IEEE Electr. Device L.* **27** (3), 142 (2006).
12. J.W. Leem, Y.T. Lee and J.S. Yu, *Opt. Quant Electron.* **41**, 605 (2010).